Ocean Sci., 22, 3795–3809, 2026
https://doi.org/10.5194/os-22-3795-2026
© Author(s) 2026. This work is distributed under
the Creative Commons Attribution 4.0 License.

Ocean Science Open Access EGU

A segmented-breakpoint measure of cross-shore sea-surface-temperature structure in the Benguela system

Albertus J. Smit[1,2] **and Neville A. Sweijd**[3]

[1]Department of Biodiversity and Conservation Biology, University of the Western Cape, Bellville, Cape Town 7535, South Africa
[2]South African Environmental Observation Network, Elwandle Coastal Node, Gqeberha 6031, South Africa
[3]School for Climate Studies, Stellenbosch University, Stellenbosch 7599, South Africa

Correspondence: Albertus J. Smit (ajsmit@uwc.ac.za)

Received: 26 May 2026 – Discussion started: 23 June 2026
Revised: 2 November 2026 – Accepted: 15 November 2026 – Published: 24 November 2026

Abstract. Satellite measures of coastal upwelling based on sea-surface temperature (SST) often compare coastal water with an offshore reference point fixed at 50 to 100 km from the coast. The surface cool tongue, however, reaches different distances offshore in different parts of the Benguela system and on different days, so no single fixed distance can be located beyond it everywhere. We fit a thermal breakpoint each day to each cross-shore SST profile by two-segment regression and accept a profile only when the fit satisfies criteria on model evidence, slope contrast, offshore baseline length, distance from the ends of the profile, and residual autocorrelation. Applying the method to five study sectors over 2015 to 2025 on two 0.05° analyses (OSTIA and OSPO), with two 0.25° analyses (AVHRR_OI and MW_OI) as resolution comparisons, we find median fitted breakpoints of 114 to 270 km. Conventional references at 50 to 100 km therefore usually fall inside the fitted inshore segment rather than beyond it. In OSTIA, the daily correlation between the fitted inshore SST contrast and the fixed-distance contrast rises from 0.06 when the reference is 50 km offshore to 0.93 when it is 500 km offshore, so moving the reference changes rather than rescales the quantity measured. Comparing the frequency with which SST profiles meet the two-segment criteria against a positive offshore Ekman-transport wind flag, the two daily classifications agree on most days but differ on about one fifth of days in the two southern study sectors. Acceptance identifies only the specified cross-shore SST structure; neither acceptance nor rejection determines the physical upwelling state. The method therefore provides a fitted thermal breakpoint x_b, an inshore SST contrast $\overline{D}_{in}$, and the frequency with which profiles meet the two-segment criteria, allowing the fitted cross-shore extent, thermal contrast, and occurrence of this SST structure to be compared among study sectors without imposing a common offshore reference.

1 Introduction

Satellite-derived sea-surface-temperature (SST) studies quantify several cross-shore thermal patterns within eastern boundary upwelling systems (EBUS), including coast–offshore temperature differences, cross-shore gradients and frontal positions, and changes in warming rate with distance from shore (Nykjaer and Van Camp, 1994; Santos et al., 2005; Benazzouz et al., 2014a; Vasquez-Cuervo et al., 2013; Seabra et al., 2019). These quantities are often interpreted as indices of upwelling intensity because wind-driven upwelling can produce cooler coastal water. In the Benguela system, warm-water intrusions associated with the Angola Current in the north and Agulhas-origin waters in the south modify SST alongside local wind-driven cooling (Salama et al., 2025). Mesoscale circulation redistributes these waters, while changes in coastal currents and horizontal heat advection contribute to SST variability along the Angolan and Namibian coasts (Hutchings et al., 2009; Tomety et al., 2024). In the strict physical sense, however, upwelling is the vertical advection of subsurface water, which a coast–offshore SST contrast neither measures nor uniquely identifies. Most contrast measures have been assessed against climatology or wind-based proxies rather

than direct estimates of vertical transport or hydrographic evidence that source water has reached the surface (Brink et al., 1983; Gordon et al., 1995; Calvert and Price, 1971; Lutjeharms and Valentine, 1987; Lamont et al., 2015). This limitation applies to all such SST contrast measures. Although determining the physical upwelling state or the boundary of upwelled water requires independent evidence, SST contrast measures are routinely used as proxies for upwelling. Their offshore reference therefore affects the quantity used to infer upwelling from SST and requires explicit justification.

Published fixed-distance implementations set the offshore reference by convention, sensitivity assessment, or correlation with wind-derived measures (Nykjaer and Van Camp, 1994; Santos et al., 2005; Marcello et al., 2011; Benazzouz et al., 2014a, b), and there are no formal criteria to set the reference per transect or latitude. Because cross-shore contrasts are an established way to gain insight into SST patterns that often accompany upwelling, the offshore reference is a substantive decision the researcher has to make: it determines which water is treated as offshore and can change both the estimated contrast and its interpretation.

Using SST is one of several approaches. Closed-isotherm-area and threshold-isotherm methods select an isotherm and report its area or extent, a fixed-distance contrast $T(d_0) - T(0)$ samples a single offshore reference point at a chosen distance d_0, and anomaly-event methods count days exceeding a percentile threshold (Marcello et al., 2011; Benazzouz et al., 2014a, b; Abrahams et al., 2021a, b). The closest published precedent for a fitted reference is the per-latitude-band offshore reference used by Benazzouz et al. (2014a) in the Canary system. Wind-based measures (Bakun, 1973; Chen et al., 2012; Lamont et al., 2018) avoid the SST-reference choice but omit, in their local form, wind-stress-curl pumping, non-local ocean response, and alongshore-advection memory (Benazzouz et al., 2014a; Bordbar et al., 2021; Hutchings et al., 2009), and describe a different feature from SST-based measures. Counts of days, events, and cumulative magnitude compare across studies only after their operational definitions are stated (Bograd et al., 2009; Iles et al., 2012; Lamont et al., 2018; Abrahams et al., 2021a, b).

The fixed-reference assumption has a quantitative consequence. Published cross-shore length scales for upwelling-affected water in the Benguela alone span ca. 50–500 km across upwelling-cell morphometry, curl-driven nearshore bands, and far-field advected footprints (Lutjeharms and Meeuwis, 1987; Bordbar et al., 2021; Pavlushin and Kubryakov, 2022; Brandt et al., 2024; Belonenko et al., 2024), so a single d_0 must sample inside the cool tongue in some locations and offshore water in others. The resulting contrast therefore compares coastal SST with different parts of the cross-shore thermal field among study sectors, so its magnitude and interpretation depend on d_0. Applications that use cross-shore SST contrasts therefore inherit the choice of reference distance, whose consequences should be stated explicitly.

Here we treat the offshore reference as a fitted property of each daily SST profile rather than as a fixed distance imposed before analysis. The two-segment regression assesses whether a profile has a detectable inshore–offshore transition and where its fitted thermal breakpoint lies on a given day. It is a statistical description of the surface SST field, not a direct measure of vertical transport or wind forcing. We analyse five study sectors from Cape Frio to Cape Peninsula over 2015–2025, then ask three linked questions: how far offshore the fitted thermal breakpoint lies, how the fitted inshore SST contrast differs from conventional fixed-distance contrasts, and how often the SST-profile and offshore Ekman-transport criteria agree.

2 Methods

2.1 Study area, SST and ancillary inputs

We prescribed five study-sector windows corresponding to long-established Benguela upwelling cells (UCs), namely Cape Frio, Walvis Bay, Lüderitz, Cape Columbine, and Cape Peninsula (Fig. 1), so that the results could be compared with earlier geographical work (Lutjeharms and Meeuwis, 1987; Hutchings et al., 2009; Kämpf and Chapman, 2016; Brandt et al., 2024). The five study sectors contain 189 curvilinear cross-shore transects generated with a boundary-conforming Laplace-potential construction (Spekreijse, 1995; Chan et al., 1994; Murray, 1996; Liu et al., 2017). The transects follow smooth streamlines connecting the coastline to an offshore contour while adapting to the shape of both boundaries. Section S1 in the Supplement gives the full mesh construction, including the coastline projection, bathymetric inputs, streamline tracing, bridge construction, and pruning rules. The regression distance x used in Sect. 2.2 is streamline arc-length, converted to coast-distance as $x_{\mathrm{coast}} = 500x/\ell$, where ℓ is streamline length.

The four SST inputs are Group for High Resolution Sea Surface Temperature (GHRSST) Level-4 analyses, namely the Operational Sea Surface Temperature and Ice Analysis (OSTIA) and NOAA Geo-Polar Blended analysis (OSPO) at ca. 0.05° (Worsfold et al., 2024; Maturi et al., 2017), and the Advanced Very High Resolution Radiometer Optimum Interpolation (AVHRR_OI) and Microwave Optimum Interpolation (MW_OI) analyses at ca. 0.25° (Banzon et al., 2016; Wentz and Meissner, 2000). ERA5 10 m winds support the wind comparison (Hersbach et al., 2020). Adjacent transects are spaced at ca. 4 km, so study-sector aggregates are spatial summaries rather than independent-transect estimates.

We construct gap-free daily SST fields from the four Level-4 SST analyses. These products fill gaps caused by cloud cover using neighbouring waters and the recent history of each field, so during extended cloudy periods, the

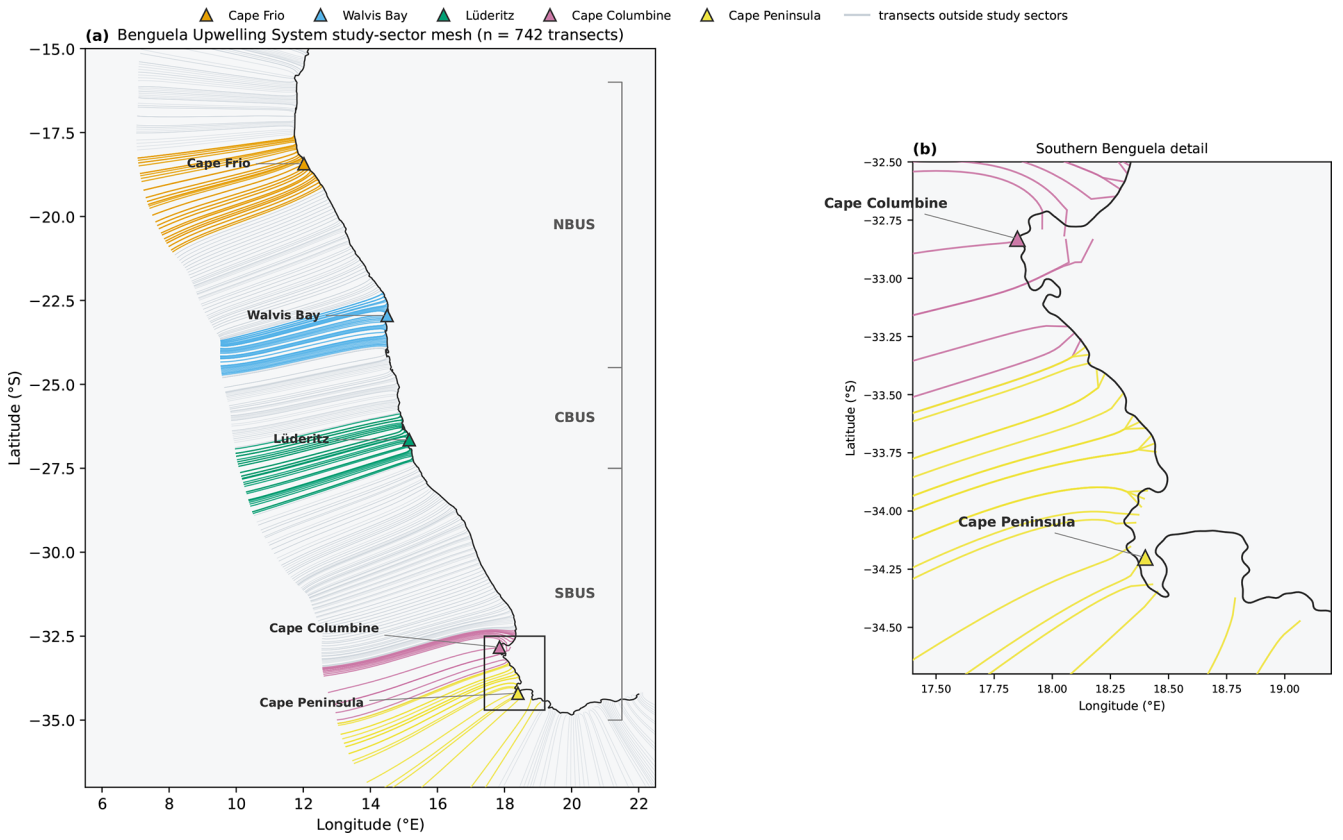

Figure 1. Five Benguela study sectors and the cross-shore mesh. Grey lines show retained transects outside the study sectors, and coloured lines show the transect sets used in the analysis. The southern Benguela inset resolves Cape Columbine and Cape Peninsula. Study-sector colours match the other figures. Brackets indicate illustrative northern (NBUS, ca. 16–24.5° S), central (CBUS, ca. 24.5–27.5° S), and southern (SBUS, ca. 27.5–35° S) regions following the mapped scheme of Salama et al. (2025). These geographical guides are separate from the five analytical study sectors and from the conventional two-subsystem division near Lüderitz at ca. 26–27° S (Hutchings et al., 2009).

resulting fields may therefore vary less than the true SST field. This concern is particularly relevant in the northern Benguela, where low cloud is persistent. A run of days meeting the SST criterion across a cloudy interval may therefore reflect persistence in the analysis rather than persistence of the feature, affecting the SST-only classification because the wind field is unaffected by cloud. We have not quantified this effect. MW_OI is largely insensitive to cloud and would be the natural control, but its resolution is too coarse to retain accepted profiles under the AR(1)-corrected criterion. Per-pixel analysis-uncertainty fields distributed with the SST products would support a quantitative treatment in future work.

2.2 Segmented-breakpoint regression

At every (product, day, transect c), one SST value per native pixel forms the cross-shore profile $T_p(x;c,t)$ (Fig. 2a). We fit a continuous two-segment piecewise-linear regression in cross-shore distance x to that profile (Fig. 2b):

$$T_p(x;c,t) = \begin{cases} \alpha_{\mathrm{in}} + \beta_{\mathrm{in}} x, & 0 \le x \le x_{\mathrm{b}}, \\ \alpha_{\mathrm{in}} + \beta_{\mathrm{in}} x_{\mathrm{b}} + \beta_{\mathrm{off}}(x - x_{\mathrm{b}}), & x_{\mathrm{b}} < x \le L. \end{cases} \quad (1)$$

Here, p, c, and t index the SST product, transect, and day, respectively, and $T_p(x;c,t)$ is SST (°C) at streamline distance x (km). The offshore limit of the fitted profile is L (km), α_{in} is the fitted SST at $x = 0$, β_{in} and β_{off} are the inshore and offshore slopes (°C km^{-1}), and x_{b} is the fitted thermal breakpoint (km) separating the two segments. The two-segment model has four free parameters $\{\alpha_{\mathrm{in}}, \beta_{\mathrm{in}}, \beta_{\mathrm{off}}, x_{\mathrm{b}}\}$, and the one-segment baseline has two, $\{\alpha, \beta\}$. Continuity at x_{b} makes the offshore intercept $\alpha_{\mathrm{off}} = \alpha_{\mathrm{in}} + \beta_{\mathrm{in}} x_{\mathrm{b}}$ a derived quantity rather than a free parameter. The offshore reference temperature used by the inshore SST contrast of Sect. 2.4 is the mean of the fitted offshore line over $x_{\mathrm{b}} < x \le L$. At each candidate x_{b}, ordinary least squares (OLS) gives the three slopes/intercepts, and the chosen x_{b} is the candidate native-pixel position that minimises the joint residual sum of squares (Fig. 2c). Because each regression is fitted per transect and the mesh is continuous along the coast, fitting does not require predefined sectors. A continuous alongshore application could therefore estimate changes in x_{b} and $\overline{D}_{\mathrm{in}}$ without imposing sector boundaries.

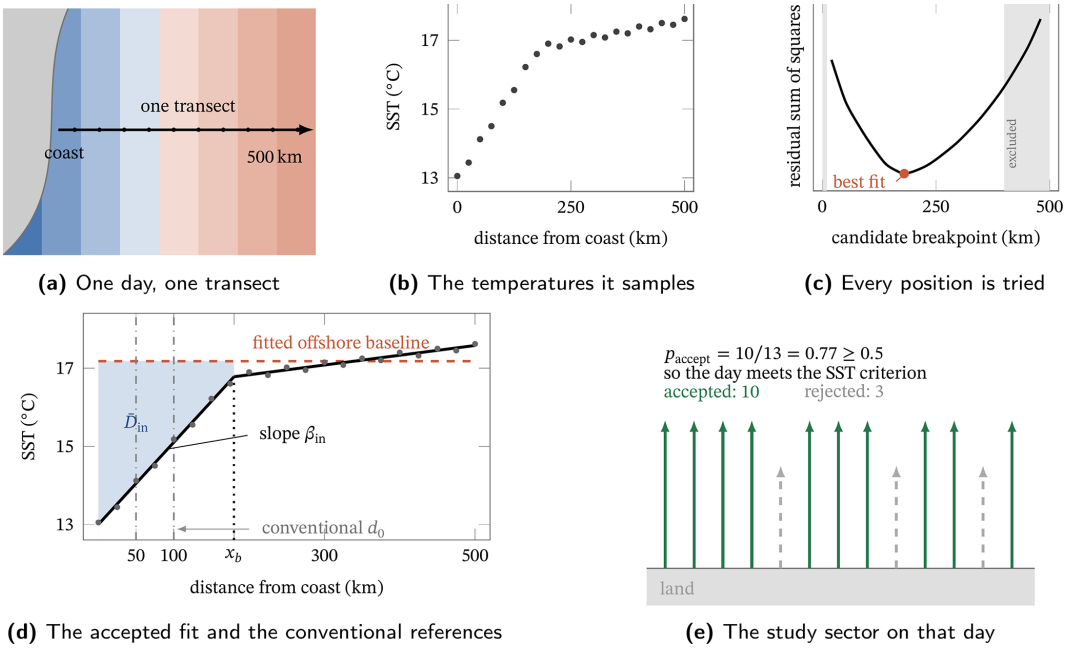

Figure 2. Calculation of a single daily breakpoint, from the temperature field to classification of the day. **(a)** One transect of the cross-shore mesh crosses the SST field on one day, and one temperature value is taken per satellite pixel along it. **(b)** These values form the cross-shore profile that is fitted. **(c)** Every candidate breakpoint position is tried and the position giving the smallest residual sum of squares is retained; the shaded bands at either end are excluded by the edge-buffer and offshore-baseline criteria. **(d)** The accepted two-segment fit, with the breakpoint x_b, the inshore slope β_{in}, the fitted offshore baseline, and the shaded inshore SST contrast $\overline{D}_{in}$; the conventional 50 and 100 km reference distances are marked and fall inside the inshore segment. **(e)** The fit is repeated at every transect in the study sector, and the accepted-profile fraction p_{accept} classifies the day. Values are illustrative and drawn for legibility.

Adjacent mesh transects are spaced at ca. 4 km, which is finer than the pixel spacing of the L4 analyses, so neighbouring transects can sample the same pixel. Two rules therefore determine what counts as an observation.

Within a transect a pixel contributes exactly one observation, and the model comparison uses that count, namely a median of ca. 91 to 101 values on OSTIA and OSPO and substantially fewer on AVHRR_OI and MW_OI (Table S1 in the Supplement). Each L4 pixel is then allocated to the first transect in which it occurs, and only transects retaining at least one pixel after deduplication contribute to the per-(study sector, product, day) population.

The rules are independent. The first fixes the sample size informing the model comparison at one transect. The second fixes which transects enter the study-sector aggregate and leaves every individual fit unchanged. A profile is then accepted only when four conditions are met.

First, to assess model-evidence, we compare the two-segment fit against a single-segment fit using the Akaike information criterion (AIC), which rewards goodness of fit and penalises each additional parameter, and require $\Delta\mathrm{AIC} = \mathrm{AIC}_{\text{one-seg}} - \mathrm{AIC}_{\text{two-seg}} \geq 4$. A difference of four units is the conventional point at which the poorer of two candidate models is regarded as having considerably less support (Burnham and Anderson, 2004). The condition checks whether the inflexion is worth the two parameters it costs.

Second, the slope-contrast condition is $|\beta_{in}|/|\beta_{off}| \geq 2.0$, meaning the inshore segment must be at least twice as steep as the offshore segment. No additional $\beta_{in} > 0$ condition is imposed, so profiles that cool offshore and profiles with opposite-sign segment slopes may also be accepted. Acceptance therefore identifies a change in gradient magnitude; a coastal-cooling interpretation requires the slope and contrast signs to be considered. Without the slope-contrast condition, a profile that warms almost uniformly offshore can satisfy the model-evidence test on a slight change in gradient.

Third, the offshore-baseline condition is $\ell - x_b \geq 100$ km, where ℓ is the streamline arc-length of the transect. It ensures that the background temperature $\widehat{T}_{bg}$ is estimated over a substantial stretch of open water rather than from the few pixels at the seaward end. The condition regularises the offshore fit, replacing a fixed reference distance d_0 with a fitted breakpoint subject to an explicit constraint on the offshore extent.

Last is an edge-buffer condition, $x_b \geq 10$ km and $\ell - x_b \geq 10$ km. A breakpoint at the coastline or the outer contour would leave one segment supported by too few points to estimate a slope, so the fit would be determined by the endpoints of the profile rather than by its shape.

This classification separates profiles with a supported steep inshore segment and a sufficiently long, weak-gradient offshore segment from profiles that are not adequately represented by that form, including gradual, nearly flat, or more complex profiles and transitions beyond the transect. It distinguishes observed SST geometries. The physical upwelling state remains undetermined in both categories.

Their influence is constrained by the threshold-sensitivity assay of Table S2, which assesses each threshold across a grid of alternatives. The study-sector descriptions of Results Sect. 3.1 hold at every tested value and are reported using the first-order autoregressive (AR(1))-corrected acceptance set described in the next subsection.

2.3 Model evidence criteria and effective sample size

Because x_b is selected over a candidate grid, we count it as a fourth free parameter and assess whether the AIC penalty accounts for the advantage gained by searching many positions. Stricter penalties have been proposed for this setting (Yao, 1988; Bai and Perron, 1998; Zhang and Siegmund, 2007). We compare AIC, small-sample AICc (Hurvich and Tsai, 1989), and BIC (Schwarz, 1978; Yao, 1988) on the Cape Columbine DJF 2020 subset across all products using the original unique-pixel count, before the AR(1) adjustment (Table S3). The unique-pixel count is ca. 90–100 in OSTIA/OSPO and 19–23 in AVHRR/MW_OI, giving AICc corrections of ca. 0.4 and 2.2–2.9 respectively; the BIC penalty per parameter is ca. 2.3 times the AIC penalty on the fine products. AIC gives the same decision as AICc and BIC for 100 % of fine-resolution and 99.5 % of coarse-resolution profiles; the stricter criteria reject only marginal coarse-product fits. The baseline decisions are therefore insensitive to the tested penalty strength.

Residual autocorrelation influences acceptance more heavily than the choice of penalty. The AIC comparison assumes that the observations are independent, but cross-shore SST profiles violate that assumption since adjacent pixels covary strongly. We quantify the dependence by fitting an AR(1) model to the OLS residuals along the unique-pixel sequence of accepted OSTIA profiles from 2020, pooling lag-1 pairs within profiles by study sector and season and applying each coefficient to all products and years. The coefficient ϕ ranges 0.884 to 0.950 with a median of 0.915, so the dependence is strong and consistent across study sectors and seasons. Each ϕ converts to an effective sample size,

$$n_{\mathrm{eff}} = n\,\frac{1-\phi}{1+\phi}, \tag{2}$$

following Chelton (1983). This conversion reduces a 95-pixel profile to approximately five effectively independent values, and we recompute the comparison score as $\mathrm{AIC}^{\star} = n_{\mathrm{eff}}\log(\mathrm{RSS}/n_{\mathrm{eff}}) + 2k$ for each model, retaining its original OLS residual sum of squares (RSS) and parameter count k. This approximates the loss of independent information; an explicit correlated-error likelihood would instead model the residual covariance. All unique pixels still contribute to the fitted coefficients. Values of n_{eff} below four indicate very limited effective information, although the score remains numerically defined for $n_{\mathrm{eff}} > 0$. We apply the same $\Delta\mathrm{AIC}^{\star} \geq 4$ screen without an additional minimum-n_{eff} requirement. AICc is used only in the separate baseline comparison above.

The correction reduces baseline acceptance by a median 24 % in OSTIA and 20 % in OSPO, and leaves no accepted profiles on AVHRR_OI or MW_OI (Table S1). The coarse products therefore serve as resolution comparisons and not as sources of breakpoint estimates, and results below use the AR(1)-corrected set. The baseline $\Delta\mathrm{AIC} \geq 4$ screen is retained only as a profile-shape comparison and as part of the threshold-sensitivity assessment.

2.4 Quantities describing the fitted cross-shore SST structure

The two-segment fit provides three literal quantities per-(product, day, transect), illustrated in Fig. 2d. The fitted thermal breakpoint x_b (km) identifies the offshore extent of the inshore steep-gradient segment. The inshore segment slope β_{in} (°C km^{-1}) is the cross-shore SST gradient over that segment, with positive values indicating warming offshore. Larger $|\beta_{\mathrm{in}}|$ indicates a steeper near-coastal SST gradient but does not identify its physical cause. The inshore SST contrast $\overline{D}_{\mathrm{in}}$ (°C) is the fitted offshore reference temperature minus the mean SST of the inshore segment:

$$\overline{D}_{\mathrm{in}} \;=\; \widehat{T}_{\mathrm{bg}} - \overline{T}_{p}^{[0,x_b]}, \tag{3}$$

where $\widehat{T}_{\mathrm{bg}}$ is the mean of the fitted offshore segment (Sect. 2.2) and $\overline{T}_{p}^{[0,x_b]}$ is the trapezoidal mean of the native-pixel SST values between the coast and the breakpoint. $\overline{D}_{\mathrm{in}}$ is dimensionally and structurally distinct from the fixed-distance contrast $T(d_0) - T(0)$ (cool inshore → positive, matching the sign of $\overline{D}_{\mathrm{in}}$). The two quantities describe different aspects of cross-shore SST structure: a segment mean relative to a fitted offshore baseline and a point contrast at a prescribed distance. Climatological aggregates per-(study sector, product, season) are the median, the 5th, and the 95th percentile across accepted days, and inter-annual variability is the analogous per-year aggregate.

2.5 Daily accepted-profile frequency

The AR(1)-corrected acceptance flag records whether an individual profile is well described by a steep inshore segment followed by a gentler offshore segment after the effective-sample correction of Sect. 2.3. It does not identify wind-driven upwelling directly. A profile can keep this SST structure after the wind relaxes, and an upwelling-favourable wind day can precede the corresponding SST response.

For each study sector and day, p_{accept} is the fraction of retained transects whose breakpoint fit is accepted. We classify the sector-level SST criterion as met when $p_{\text{accept}} \geq 0.5$, i.e. when at least half of the retained transects meet the two-segment criteria (Fig. 2e). The threshold expresses a majority rule. Repeating the classification at 0.3 and 0.7 preserves the broad ranking among study sectors (Table S4).

Before periods are defined, we bridge one sub-threshold day flanked by days meeting the criterion. A met–not-met–met sequence therefore becomes a three-day run, whereas two sub-threshold days terminate a period. Runs of at least three days are counted as periods. We report the annual count of days meeting the criterion, the number of periods, and the annual sum of daily-median $\overline{D}_{\text{in}}$ over those days.

These summaries follow the July-to-June year, single-day bridging rule, and minimum three-day period used by Lamont et al. (2018); SST-anomaly studies use related event counts (Abrahams et al., 2021a, b). The product-specific accepted-profile fractions and annual summaries are shown in Figs. S1 and S2 in the Supplement. Under the AR(1)-corrected criterion they are reported for OSTIA and OSPO only, while AVHRR and MW_OI are kept in Table S1 as product-resolution references.

2.6 Comparison with fixed-distance SST contrasts and offshore Ekman transport

We compare $\overline{D}_{\text{in}}$ with the conventional fixed-distance SST contrast $T(d_0) - T(0)$ in the cool-coastal-positive sign convention, computed at $d_0 \in \{50, 100, 200, 500\}$ km. These distances span the curl-driven nearshore band, Benguela upwelling-cell SST extents, and the far-field advected footprint of upwelled water (Lutjeharms and Meeuwis, 1987; Bordbar et al., 2021; Pavlushin and Kubryakov, 2022; Brandt et al., 2024; Belonenko et al., 2024). The fixed-distance contrast and $\overline{D}_{\text{in}}$ describe different aspects of cross-shore SST structure: a point contrast at d_0 and a segment mean relative to a fitted offshore baseline. Their Pearson r describes co-variability and does not calibrate one quantity against the other. We denote by r_{d_0} the daily Pearson correlation between $\overline{D}_{\text{in}}$ and $T(d_0) - T(0)$ over all accepted days, with r_{50} as the value at $d_0 = 50$ km. We also report $P(d_0 < x_{\text{b}})$ per-(study sector, product, season) and threshold setting, with block-bootstrap intervals.

We compute offshore Ekman transport from ERA5 daily-mean 10 m winds following its application to coastal upwelling by Bakun (1973). At each study-sector reference location, wind stress is projected onto a sector-level alongshore unit vector oriented equatorward, using the coordinate construction of Lamont et al. (2018). Writing τ_{along} for that component, offshore Ekman transport per unit length of coast is $-\tau_{\text{along}}/(\rho_w f)$, where ρ_w is held constant at $1025\,\text{kg}\,\text{m}^{-3}$ and f is the Coriolis parameter. Density is prescribed, so no salinity observations or equation-of-state calculation are used. In the southern hemisphere f is negative, so equatorward alongshore stress gives positive offshore transport. The sector direction is obtained by normalising the component-wise median of the equatorward vectors perpendicular to its coastal transects. A day meets the wind criterion when its daily-mean offshore Ekman transport is positive. This sign rule differs from the wind-speed threshold of Lamont et al. (2018); their study is cited for the coordinate construction and the July-to-June aggregation and event-linking operations used here. This local wind measure omits wind-stress-curl pumping and geostrophic transport, including potentially important contributions in the southern Benguela. We retain offshore Ekman transport to compare SST structure with local wind forcing. We compare daily SST and wind classifications and, separately, compare annual sums of $\overline{D}_{\text{in}}$ on days meeting the SST criterion with annual cumulative offshore Ekman transport. Annual correlations use available (product, study sector, year) combinations.

2.7 Agreement between SST and wind classifications

The SST criterion and the daily offshore Ekman-transport criterion (Sect. 2.6) are two classifications of the same day, neither of which is the truth, so the comparison is one of agreement rather than validation. Per-(study sector, product, season), we report six agreement statistics for the matched pair, namely balanced accuracy, sensitivity and specificity taken in both directions, raw agreement p_o, Cohen's κ, and the Matthews correlation coefficient (MCC) (Matthews, 1975; Byrt et al., 1993; Chicco and Jurman, 2020) (Table S5). No single statistic characterises a 2×2 agreement table completely, which is why we report the set.

For the paired classification (both criteria met, neither met, SST criterion only, wind criterion only), we create a date-shuffled-within-season null baseline. The shuffle preserves the number of positive days returned by each classification and removes their day-to-day alignment. For each (study sector, product, season), we permute the SST daily flags within season, recompute every agreement statistic, and repeat this process 1000 times. The central 95 % of the shuffled results is the range expected if the two classifications have the same seasonal prevalence but no daily correspondence. We report this interval alongside the observed statistic (Table S5). The null tests whether the observed agreement exceeds that chance baseline at the within-season scale; it does not test mechanism.

2.8 Uncertainty in study-sector summaries and individual breakpoints

Two distinct uncertainty questions arise. The first concerns study-sector summaries, such as the median breakpoint position or the fraction of days on which only the SST criterion is met. These summaries are computed over many transects, but adjacent transects are spaced at ca. 4 km and sample overlapping water, so they do not contain independent informa-

tion. Treating each transect as an independent observation would make the summaries appear more precise than they are. We therefore resample in contiguous alongshore blocks of 25 and 50 km rather than resampling individual transects, since a block preserves the alongshore correlation within it and the blocks can be treated as approximately independent of one another. Where the summary is annual or seasonal, years and seasons are resampled as blocks for the same reason. Reported intervals are 1000-replicate percentile intervals.

The second concerns an individual profile. A study-sector interval does not show whether one profile determines its breakpoint well, so we estimate this separately. For a stratified sample of 4000 accepted profiles, we resample its pixels with replacement, refit the breakpoint 1000 times, and record the fitted-position spread. A broad or bimodal distribution indicates an ambiguous solution. We flag bimodality when a Gaussian kernel density estimate has two peaks with prominence at least 0.1 times the maximum and separated by more than 50 km. Table S6 and Fig. S4 report the interval-width and bimodality summaries.

Table 1. Climatological annual medians of the fitted cross-shore SST quantities per study sector and fine-resolution product, computed on the AR(1)-corrected accepted-profile set and averaged over the four austral seasons across 2015–2025. AVHRR and MW_OI are excluded because the AR(1)-corrected criterion returns no accepted coarse-product profiles in the per-(study sector, product, season) tests (Table S1).

Study sector	Product	$\overline{D}_{\mathrm{in}}$ (°C)	x_{b} (km)	β_{in} (°C km^{-1})
Cape Frio	OSTIA	2.08	153	0.021
	OSPO	2.05	159	0.020
Walvis Bay	OSTIA	2.54	264	0.017
	OSPO	2.43	270	0.015
Lüderitz	OSTIA	3.21	156	0.034
	OSPO	3.16	159	0.032
Cape Columbine	OSTIA	2.55	175	0.030
	OSPO	2.41	181	0.027
Cape Peninsula	OSTIA	2.53	114	0.043
	OSPO	2.16	114	0.042

3 Results

3.1 Study-sector SST characterisation across four products

Our main findings are based on OSTIA and OSPO, the two fine-resolution L4 analyses that retain usable inshore SST in every study sector and substantial accepted-profile populations after AR(1) residual decorrelation. After AR(1) correction (Methods Sect. 2.3), OSTIA and OSPO lose a median 24 % and 20 % of baseline acceptance respectively across their per-(study sector, product, season) strata; Table S1 gives the pre- and post-correction p_{accept} values. AVHRR and MW_OI retain no accepted profiles in any per-(study sector, product, season) stratum, so they offer only product-resolution insight rather than breakpoint estimates. OSTIA and OSPO reveal study-sector-specific breakpoint distributions (Table 1). The annual median fitted breakpoint x_{b} spans 114–270 km across the five study sectors, namely 114 km at Cape Peninsula, 153–159 km at Cape Frio, 156–159 km at Lüderitz, 175–181 km at Cape Columbine, and 264–270 km at Walvis Bay. Per-(study sector, product) annual medians of the inshore SST contrast $\overline{D}_{\mathrm{in}}$ range 2.05–3.21 °C, with the lower bound at Cape Frio with OSPO and the upper bound at Lüderitz with OSTIA. The per-(study sector, product, season) breakdown of x_{b}, $\overline{D}_{\mathrm{in}}$, β_{in}, and the four fixed-distance contrasts $T(d_0) - T(0)$ is in Table S7.

Per-profile x_{b} identifiability, namely the width of the bootstrap interval on an individual accepted fit, is distinct from the study-sector median summaries. On the stratified random sample of 4000 accepted 2020 profiles (Sect. 2.8; Table S6 and Fig. S4), the per-profile 90 % bootstrap CI on $\hat{x}_{\mathrm{b}}$ has a median width of 22.5 km pooled across the five study sectors, 90.8 % of profiles have widths below 100 km, and 5.4 % are flagged bimodal. Median CI width is comparable across the sectors (21.5–27.4 km), and OSPO has systematically narrower per-profile intervals than OSTIA in the corresponding per-(study sector, product, season) strata (median 17–23 km in OSPO versus 22–28 km in OSTIA). Bimodality fractions range 0.03–0.08 per study sector. The typical accepted profile therefore has a well-determined breakpoint, with a small tail of profiles ($\sim$ 5 %–10 %) whose objective function has either a wide CI or a secondary inflexion. The study-sector medians do not transfer per-profile uncertainty, but the assessment supports their interpretation as spatial summaries rather than averages over widely uncertain individual fits.

A rejected profile fails at least one of the ΔAIC, slope-ratio, offshore-segment-length, or edge-buffer criteria of Sect. 2.2. Rejection therefore shows that the profile lacks a detectable two-segment structure on that day at that transect; it does not establish the absence of upwelling. A cool tongue that extends beyond the outer contour, a diffuse frontal transition, or broad curl-driven uplift can occur without the break of slope required by the criteria. The per-(day, transect) rejection rate in the archived OSTIA representative-profile population varies by more than an order of magnitude across the five study sectors; examples of accepted and rejected profiles are shown in Fig. S5. Pooled across DJF and JJA, rejection is 8.9 % at Cape Frio, 30.5 % at Walvis Bay, 0.7 % at Lüderitz, 3.5 % at Cape Columbine, and 23.4 % at Cape Peninsula. Walvis Bay has the highest rejection rate, the largest accepted x_{b} (259 km in the DJF–JJA OSTIA population), and the shallowest accepted β_{in} (+0.014 °C km^{-1}).

Rejected profiles in four study sectors retain a gradual cross-shore gradient (ca. $+0.004$ to $+0.011\,°C\,km^{-1}$ when DJF and JJA are pooled), so the criteria mostly screen profiles that warm monotonically offshore without a distinct inflexion. Cape Peninsula is the exception, with a near-zero rejected slope (pooled ca. $+0.001\,°C\,km^{-1}$), consistent with a thermally featureless cross-shore field.

The study-sector descriptions above use the baseline acceptance thresholds of Sect. 2.2, and the threshold-sensitivity assay (Table S2) shows that they are insensitive to those choices. All five OSTIA study sectors continue to satisfy $P(x_b > 50\,km) \geq 0.5$ at every tested value of every threshold, so the conclusion that conventional 50 km references sit inside the fitted inshore segment does not depend on the baseline thresholds. The Lüderitz annual r_{50} keeps a negative sign in OSTIA across the grid (-0.16 to -0.14). Per-(study sector, product) acceptance fractions are most sensitive to the offshore-baseline criterion, so at 200 km, Walvis Bay OSTIA/OSPO acceptance falls from 0.77 to 0.52/0.48 (33 %/36 % relative loss), while the other four study sectors lose at most 6 % on the fine-resolution products. The 100 km baseline is therefore a compromise between offshore-baseline length and accepted-profile coverage in the broader study sectors.

3.2 Breakpoint position and fixed-distance comparison

The scatter plots test whether the relationship between $\overline{D}_{in}$ and $T(d_0) - T(0)$ depends on the fixed reference distance; they do not calibrate one quantity against the other or imply that the two can be substituted. In the AR(1)-corrected OSTIA set, the pooled correlation rises from $r = 0.06$ at 50 km to 0.44, 0.79, and 0.93 at 100, 200, and 500 km respectively (Fig. 3; Table S8). The fitted breakpoint distributions explain this dependence (Fig. 4). At 50–100 km the breakpoint usually lies offshore of the reference distance, so the reference point is still inside the fitted inshore segment. At 200 km the result depends on study sector, and in OSTIA, $P(x_b \leq 200\,km)$ spans 0.32 at Walvis Bay to 0.98 at Cape Peninsula. Only 500 km is offshore of the breakpoint in every study sector in OSTIA and OSPO.

At Lüderitz the annual aggregate r_{50} in OSTIA is -0.16, so across the year the fitted inshore drawdown and the 50 km fixed-distance contrast vary in opposite senses. The interval on that estimate is wide. Because adjacent transects are not independent, we resample in alongshore blocks of 50 km, and the block-bootstrap 95 % interval goes from -0.21 to $+0.13$ (Table S9). The annual sign inversion therefore holds in the point estimate while the interval encompasses zero, and we do not treat it as established.

Seasonal aggregates resolve the pattern more sharply. Forty (study sector, product, season) combinations were tested, and at that number some will return a negative r_{50} by chance, so we control the false discovery rate by the Benjamini–Hochberg procedure. This procedure converts each p value into an adjusted q value that bounds the expected proportion of false positives among the significant combinations. Four negative cases pass at $q < 0.001$, namely Cape Peninsula in MAM (March–May) on both fine-resolution products, Lüderitz in MAM on OSPO, and Walvis Bay in SON (September–November) on OSPO. Cape Frio does not support a negative seasonal claim in the AR(1)-corrected accepted dataset. When r_{50} is negative, days with a stronger 50 km fixed-distance contrast coincide with days on which $\overline{D}_{in}$ weakens.

3.3 Agreement between SST and wind classifications

The AR(1)-corrected acceptance flag, aggregated to the daily accepted-profile fraction p_{accept}, gives a binary study-sector classification in OSTIA and OSPO. The annual median number of days meeting the SST criterion is 339/330 at Lüderitz and 332/322 at Cape Columbine in OSTIA/OSPO respectively (Table S10). Cape Frio is intermediate, with medians of 221/228 d. Walvis Bay has medians of 118/117 d and several years whose annual median p_{accept} is near zero. Cape Peninsula has pronounced summer maxima in p_{accept} alternating with winter minima.

Paired SST and wind daily classifications separate into four classes of unequal size (Fig. 5). Each matched study-sector–product–day is assigned to both criteria met, neither met, SST criterion only, or wind criterion only. Both criteria are met on a mean seasonal fraction of 0.83 at Lüderitz in both products, while wind-criterion-only days dominate at Walvis Bay in MAM and JJA (Table S5). In the two southern study sectors, SST-criterion-only days account for a mean 0.23–0.24 of matched days at Cape Columbine and 0.17–0.19 at Cape Peninsula in OSTIA/OSPO. The pooled fraction is 0.20–0.21 with alongshore 25–50 km block-bootstrap 95 % intervals of ca. 0.16–0.22 (Table S9). These fractions are descriptive classification outcomes and do not identify the physical mechanism of the SST-only days.

4 Discussion

The segmented-breakpoint regression gives a per-day, per-transect fitted thermal breakpoint that varies systematically among the five Benguela study sectors and that usually lies offshore of the conventional 50–100 km fixed references. We discuss this finding around three points. First, the study-sector dependence of x_b means that no single d_0 matches every sector. Second, the daily Pearson correlation between $\overline{D}_{in}$ and the 50 km fixed-distance contrast can be weak or negative, with the Lüderitz annual point estimate negative but not significant by block bootstrap. Third, the paired SST–wind classification gives a four-class daily decomposition, with SST-criterion-only fractions near one fifth in the two southern study sectors.

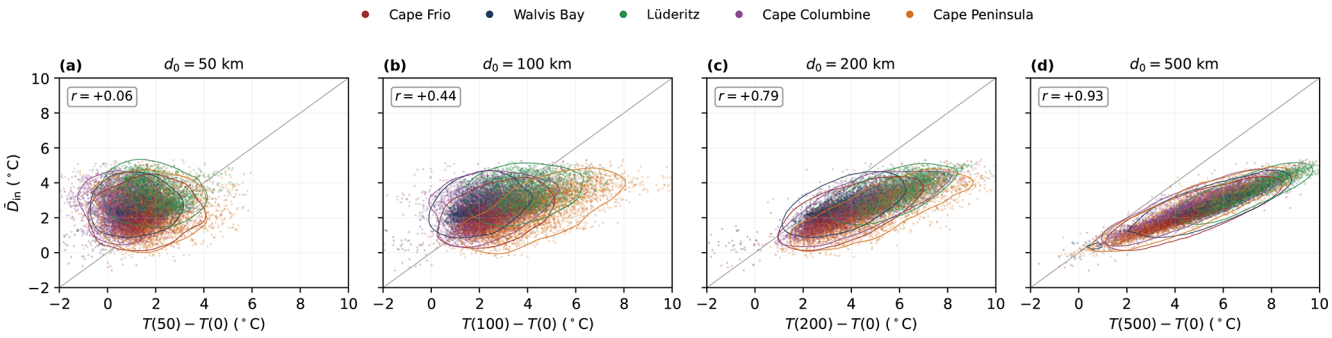

Figure 3. OSTIA daily-median inshore SST contrast $\overline{D}_{\mathrm{in}}$ on the AR(1)-corrected accepted set (y-axis, expressed in °C) against the fixed-distance contrast $T(d_0) - T(0)$ (x-axis, expressed in °C). Daily medians are computed across study-sector transects. The four panels use $d_0 = 50$, 100, 200, and 500 km to show how the relationship changes with reference distance. The five study sectors are colour-coded, the grey line is the 1 : 1 reference, and Pearson r is annotated in each panel. The full per-(study sector, product, season) correlation table is in Table S8.

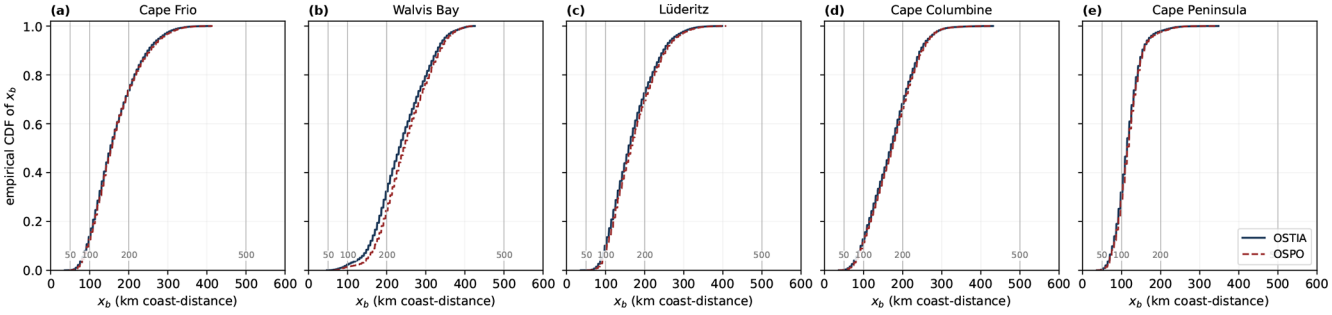

Figure 4. Empirical cumulative distribution of the fitted breakpoint position x_{b} in each study sector across the 11-year analysis window on the AR(1)-corrected accepted set, reported in km coast-distance via the linear streamline-stretch approximation of Methods Sect. 2.1. Five panels arranged horizontally show the product-specific empirical CDFs as line styles: OSTIA solid and OSPO dashed. Vertical grey lines mark the four reference distances $d_0 = 50$, 100, 200, 500 km used in the analysis.

4.1 Physical basis and scope of the two-segment description

The two-segment form describes the *shape* of the cross-shore SST profile. Coastal upwelling places recently surfaced water in a band against the coast, separated from offshore surface water by a frontal transition, and the cross-shore temperature gradient is steeper within the band than beyond it. de Szoeke and Richman (1984) show that wind mixing of a mixed layer with a strong horizontal gradient can sharpen this transition, while its position depends on wind history and stratification. A fitted breakpoint therefore estimates a quantity that theory predicts should vary from day to day. We do not claim that the two-segment fit recovers the frontal position in a dynamical sense, since establishing that correspondence would require hydrographic sections across the fitted breakpoint.

The acceptance criteria select a steep inshore gradient followed by a weaker offshore gradient. Curl-driven upwelling can act across a broad offshore band without producing that shape, so the method may reject such a profile or place its breakpoint far offshore. A rejected profile can also contain recently upwelled water when the cool tongue extends beyond the outer contour or when the frontal transition is too diffuse to satisfy the slope criterion.

4.2 Conventional fixed-distance references mis-position the fitted thermal reference

SST-based descriptions follow two related "lineages". Closed-isotherm and isotherm-area methods delineate a two-dimensional region, including the Benguela definitions of Lutjeharms and Meeuwis (1987) and Hagen et al. (2001). They quantify the area enclosed by the coast and a selected isotherm, combining extent and intensity while remaining sensitive to the threshold. Fixed-distance contrasts instead reduce a cross-shore profile to the difference between coastal SST and an offshore reference. The segmented regression belongs to this contrast lineage and addresses its fixed-reference assumption by fitting the cross-shore transition. It estimates where an areal outline would cross a transect, but it does not displace the area-based methods. The two approaches answer different questions, and the choice

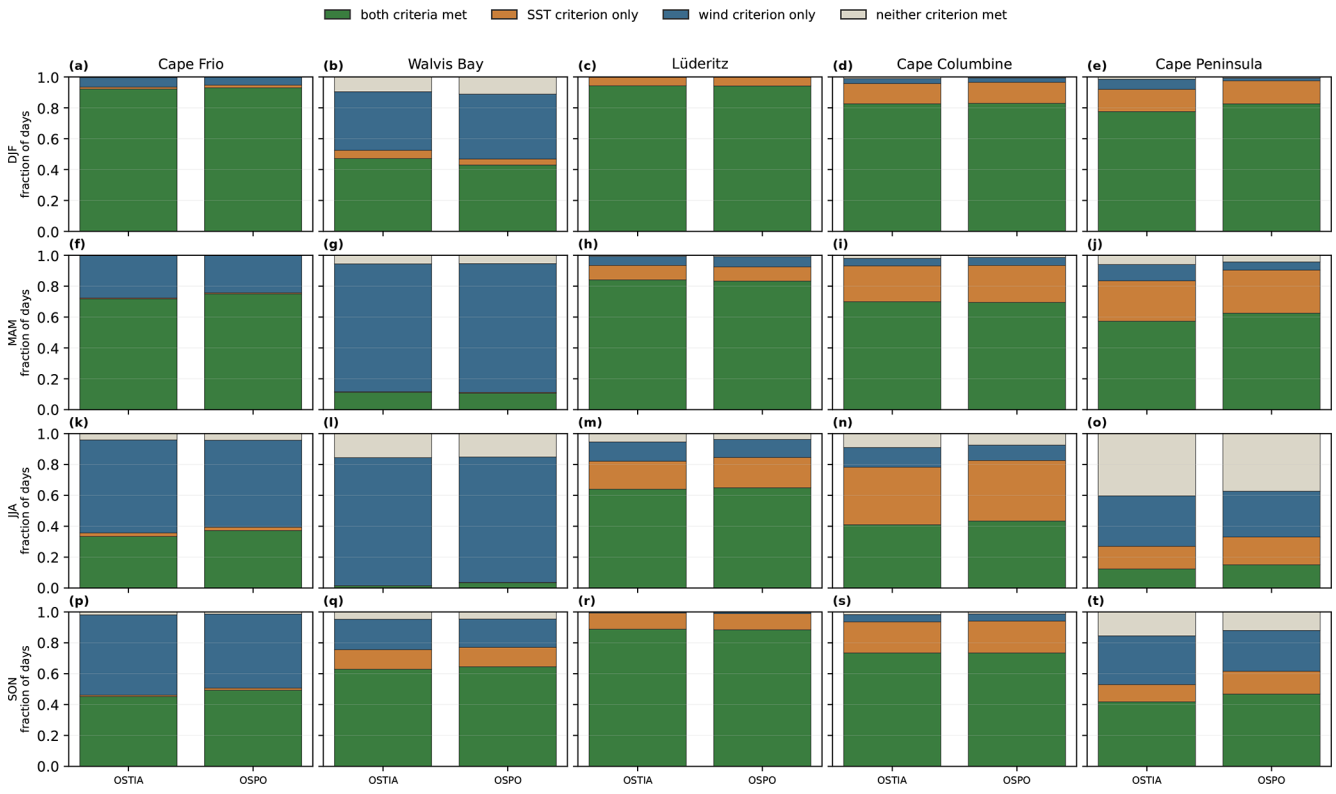

Figure 5. Per-(study sector, product, season) four-class decomposition of daily SST–wind classification on the AR(1)-corrected OSTIA and OSPO accepted set, shown as a season-by-study-sector grid with product bars within each panel. The SST criterion is met when $p_{\mathrm{accept}} \geq 0.5$ (Methods Sect. 2.5), and the wind criterion is met when daily-mean offshore Ekman transport is positive. ERA5 wind stress is projected onto the local alongshore unit vector oriented equatorward, using the coordinate construction of Lamont et al. (2018) (Methods Sect. 2.6). The four classes are both criteria met, neither met, SST criterion only, and wind criterion only.

follows from whether the target quantity is an areal footprint or a cross-shore length scale and thermal contrast.

The Benguela has no single literature-standard offshore reference distance for SST-based descriptions. Published length scales span ca. 100–380 km across established upwelling cells in Lutjeharms and Meeuwis (1987), 70–250 km in later SST morphometric work (Pavlushin and Kubryakov, 2022; Brandt et al., 2024), 50–150 km for wind-stress-curl-driven upwelling (Bordbar et al., 2021), and advected footprints up to ca. 300–500 km in eddy-resolving tracking (Belonenko et al., 2024). A single fixed reference will therefore lie inshore of the breakpoint in some study sectors and offshore in others, so $T(d_0) - T(0)$ will differ from the fitted inshore SST contrast except where d_0 happens to match the fitted transition. For applications that build on a cross-shore SST contrast, the discrepancy scales with the distance between the fixed reference and the fitted breakpoint and can change sign among study sectors. Contrast methods remain useful descriptors of SST patterns associated with upwelling, but their physical and comparative interpretation depends on the offshore reference. Its location therefore requires an explicit rationale and sensitivity assessment.

The median fine-product breakpoint position, 114–270 km across the five study sectors (Sect. 3.1, Table 1, and Fig. 4), overlaps Benguela upwelling-cell and curl-driven reference bands but lies inshore of the far-field advected-footprint scale. The strong correlation between $\overline{D}_{\mathrm{in}}$ and $T(500) - T(0)$ in OSTIA pooled across study sectors ($r = 0.93$ in Sect. 3.2) is therefore a comparison between related quantities, not proof that a 500 km fixed point is mechanistically preferable. $\overline{D}_{\mathrm{in}}$ averages over a fitted inshore segment, whereas $T(d_0) - T(0)$ samples one fixed offshore point. At Lüderitz, Cape Peninsula, and Walvis Bay, the seasonal correlation between $T(50) - T(0)$ and $\overline{D}_{\mathrm{in}}$ can change sign across season and product (Sect. 3.2). The reversal occurs because the 50 km reference lies inside the fitted inshore segment on most accepted profiles.

Walvis Bay defines a practical limit of the acceptance criteria. It has the broadest fitted inshore segment, the shallowest accepted inshore slope, and the highest rejection rate; raising the offshore-baseline requirement from 100 to 200 km reduces OSTIA/OSPO acceptance from 0.77 to 0.52/0.48 while the other study sectors lose at most 6 % (Sect. 3.1). Its broad shelf contrasts with the narrow shelf and persistent, intense upwelling at Lüderitz, where strong winds

favour offshore advection (Hutchings et al., 2009; Kämpf and Chapman, 2016). Yet the median breakpoint at Lüderitz lies inshore of that at Walvis Bay (Table 1), showing that stronger upwelling need not imply a farther-offshore thermal transition. The predominance of wind-criterion-only days in MAM and JJA is therefore consistent with the rejection of broad profiles whose offshore transition is weakly expressed, rather than showing that SST structure is absent. It does not determine whether physical upwelling occurred. The diffuse configuration described by Hutchings et al. (2009) and Lutjeharms and Meeuwis (1987) supports this interpretation. Shelf geometry and frontal dynamics may influence these regional differences, while Cape Frio is also exposed to warm-water advection near the Angola–Benguela front (Hutchings et al., 2009; Kämpf and Chapman, 2016). Resolving their contributions to individual breakpoints would require independent hydrographic and current observations.

4.3 Days meeting only the SST criterion in the southern study sectors

At Cape Columbine and Cape Peninsula, the SST criterion is met on ca. one fifth of days when the offshore Ekman-transport criterion is not (Sect. 3.3). Candidate explanations include wind-stress-curl pumping (Bordbar et al., 2021), alongshore advection from upstream upwelling cells (Hutchings et al., 2009; Benazzouz et al., 2014a), mesoscale retention and horizontal advection associated with Agulhas-origin eddies and filaments (Hutchings et al., 2009; Kämpf and Chapman, 2016), non-local ocean response to remote forcing (Benazzouz et al., 2014a), and timing mismatch between sub-daily wind variability and daily-mean Level-4 SST. Persistence introduced by Level-4 interpolation during cloudy intervals is an additional observational explanation, particularly in the northern Benguela. We list these as plausible explanations but do not diagnose their relative contributions. ERA5 is a reanalysis whose near-coastal winds depend on model resolution, orography, and coastline representation, so agreement compares model-mediated SST and wind products rather than either classification against truth. Cape Peninsula's pronounced summer maxima in p_{accept} alternate with winter minima and are consistent with the stop-start pulsed-upwelling regime described for the southern Benguela (Lamont et al., 2018; Hutchings et al., 2009; Kämpf and Chapman, 2016).

4.4 Interpretive scope

The fitted breakpoint x_{b}, the inshore SST contrast $\overline{D}_{\mathrm{in}}$, the accepted-profile fraction p_{accept}, fixed-distance SST contrasts, closed-isotherm regions (Lutjeharms and Meeuwis, 1987; Hagen et al., 2001), SST gradients (Benazzouz et al., 2014a; Vasquez-Cuervo et al., 2013), anomaly events (Abrahams et al., 2021a, b), and offshore Ekman transport (Bakun, 1973; Lamont et al., 2018) each describe a feature of the surface SST or wind field that is consistent with coastal upwelling. We use the established SST- and wind-based quantities as comparative benchmarks, not as validation against a physical standard, because they describe different features. None directly measures vertical velocity, source depth, or volume flux. At the per-(study sector, day, transect) scale used here, independent validation would require hydrographic observations, including the South Atlantic Central Water signature (Lutjeharms and Valentine, 1987; Lamont et al., 2015), or complementary measurements of currents, sea level, wind-stress curl, and the surface heat budget.

The breakpoint quantities separately describe the fitted extent, thermal contrast, and occurrence of the specified SST structure, which a fixed-distance contrast does not distinguish. Combined with offshore Ekman transport, they separate days when local upwelling-favourable wind and the two-segment SST structure coincide from days when only one criterion is met. This comparison reveals study-sector and seasonal differences in wind–SST co-occurrence that either quantity alone would conceal and identifies cases in which response timing, alongshore advection, curl-driven uplift, mesoscale retention, or surface heat exchange may require investigation. It does not distinguish among these processes.

We therefore use literal descriptions throughout. The breakpoint is a fitted thermal breakpoint in a cross-shore SST profile; $\overline{D}_{\mathrm{in}}$ is an inshore SST contrast against the fitted offshore baseline; $T(d_0) - T(0)$ is a fixed-distance SST contrast; and the wind quantity is offshore Ekman transport. These terms state what is calculated without assigning a new name to the method or implying that the fitted breakpoint is the physical edge of upwelled water.

4.5 Limitations and forward look

The analysis focuses on five Benguela study sectors where the breakpoint regression consistently accepts profiles from the fine-resolution products. We do not yet test weaker or transitional parts of the coast such as Namaqualand, north of Cape Frio, or the Agulhas-influenced coast south of Cape Peninsula. AVHRR and MW_OI are useful for documenting product-resolution sensitivity, but they are not used for inference because the AR(1)-corrected criterion gives zero accepted coarse-product profiles in the tested per-(study sector, product, season) strata. With independent physical validation, the fitted extent and inshore SST contrast could support an SST-based upwelling index for assessing long-term coastal changes under warming and altered upwelling-favourable winds.

Bathymetric controls on x_{b}, namely whether the fitted breakpoint co-locates with the shelf break or with another bathymetric feature, are outside the scope of the present analysis. A shelf-break comparison would require deriving shelf-break distance along the same operational transect mesh.

The fitted-reference method replaces a fixed offshore-reference threshold with explicit statistical and profile-

acceptance thresholds, but it does not remove thresholds. A self-contained assay over $p_{\mathrm{accept}} \in \{0.3, 0.5, 0.7\}$ preserves the broad ranking of annual accepted-day counts: Lüderitz and Cape Columbine remain near year-round, Walvis Bay has the lowest count, and Cape Peninsula is the most threshold-sensitive southern study sector (Table S4). Counts based on wind, SST anomalies, weekly frequency of occurrence, or profile acceptance likewise depend on their stated definitions.

5 Conclusions

First, a daily two-segment regression applied to cross-shore SST profiles gives a fitted thermal breakpoint x_{b}, an inshore SST contrast $\overline{D}_{\mathrm{in}}$, and an AR(1)-corrected acceptance flag. Across the five Benguela study sectors in 2015–2025, median x_{b} on fine-resolution products spans 114–270 km, so the conventional 50–100 km fixed offshore references fall inside the fitted inshore segment on most accepted profiles.

Second, the choice of reference distance can reverse or weaken the relationship with $\overline{D}_{\mathrm{in}}$. At Lüderitz, the annual aggregate point estimate is negative ($r_{50} = -0.16$, block-bootstrap 95 % interval $[-0.21, +0.13]$) but the interval encompasses zero. After Benjamini–Hochberg adjustment for the 40 seasonal tests, negative seasonal r_{50} values remain in Cape Peninsula MAM on both fine products and in Lüderitz MAM and Walvis Bay SON in OSPO. Only the 500 km reference lies beyond the breakpoint in every study sector, but its correlation with $\overline{D}_{\mathrm{in}}$ does not establish 500 km as a mechanistically correct reference.

Third, the paired SST–wind classification gives four daily outcomes rather than a single binary comparison, and SST-criterion-only days account for ca. one fifth of matched days in the two southern study sectors in OSTIA/OSPO. Cross-shore SST contrasts remain useful for examining surface patterns that often accompany upwelling, but their magnitudes vary among study sectors and with reference distance. Our 2015–2025 window is not used to estimate trends.

Fourth, x_{b}, $\overline{D}_{\mathrm{in}}$, and p_{accept} are statistical descriptions of cross-shore SST structure. Used alongside established SST- and wind-based quantities, they provide a complementary description of how the observed cross-shore SST field varies among study sectors. They do not independently establish the physical mechanism, and validation against hydrography, currents, sea level, wind-stress curl, or heat-flux evidence remains a separate empirical task.

The practical consequence is that studies using Benguela SST contrasts should report the offshore reference and spatial scale, explain how the reference was selected, and test whether the conclusions persist across plausible distances. A 50 km contrast, a 500 km contrast, and $\overline{D}_{\mathrm{in}}$ describe different parts of the surface thermal field. Substituting one for another changes the inferred spatial ranking, persistence, and SST–wind agreement.

Code and data availability. The four operational SST products, namely OSTIA, OSPO Geo-Polar Blended, AVHRR OI, and MW OI, are publicly available through National Aeronautics and Space Administration (NASA) Earthdata:

- GHRSST Level 4 OSTIA Global Historical Reprocessed Foundation Sea Surface Temperature Analysis (https://doi.org/10.5067/GHOST-4RM02, NASA/JPL, 2023).
- GHRSST Level 4 OSTIA global foundation sea surface temperature analysis (GDS version 2) (https://doi.org/10.5067/GHOST-4FK02, UKMO, 2013).
- GHRSST Level 4 OSPO Global Foundation Sea Surface Temperature Analysis (GDS version 2) (https://doi.org/10.5067/GHGPB-4FO02, Maturi et al., 2014).
- GHRSST Level 4 AVHRR_OI Global Blended Sea Surface Temperature Analysis (GDS2) (https://doi.org/10.5067/GHAAO-4BC21, NASA/JPL, 2020)
- GHRSST Level 4 MW_OI Global Foundation Sea Surface Temperature analysis version 5.1 from REMSS (https://doi.org/10.5067/GHMWO-4FR51, NASA/JPL, 2017).

ERA5 hourly 10 m winds are available from the Copernicus Climate Data Store (ERA5 hourly data on single levels, https://doi.org/10.24381/cds.adbb2d47, Hersbach et al., 2023, 2020). The breakpoint-regression formulation, the candidate-grid search, the acceptance criteria, the AR(1)-corrected acceptance rule, the product-specific native-pixel sampling rules, and the mesh construction are stated in full in Methods Sect. 2.1–2.3 and Sect. S1. The processing scripts, study mesh and sector definitions, derived profile and daily summaries, AR(1)-corrected tables, bootstrap diagnostics, and reproducibility instructions are archived in Zenodo (version 1.0.0; Smit and Sweijd, 2026; https://doi.org/10.5281/zenodo.24306305). The code repository is https://github.com/ajsmit/segmented-breakpoint-sst-benguela (last access: 19 November 2026). The archive documents the external SST and ERA5 inputs required for a complete rerun.

Supplement. The supplement related to this article is available online at https://doi.org/10.5194/os-22-3795-2026-supplement.

Author contributions. AJS designed the analysis, wrote the code, processed the data, produced the figures and tables, and wrote the first manuscript draft. NS contributed to the conceptual framing, Benguela interpretation, funding acquisition, and manuscript revision. Both authors reviewed and approved the submitted manuscript.

Competing interests. The contact author has declared that neither of the authors has any competing interests.

Disclaimer. Publisher's note: Copernicus Publications remains neutral with regard to jurisdictional claims made in the text, published maps, institutional affiliations, or any other geographical rep-

resentation in this paper. The authors bear the ultimate responsibility for providing appropriate place names. Views expressed in the text are those of the authors and do not necessarily reflect the views of the publisher.

Acknowledgements. We thank the data providers whose operational products this work depends on: the Group for High Resolution Sea Surface Temperature (GHRSST) for the Level-4 SST analyses (the UK Met Office, the NOAA Office of Satellite and Product Operations, the NOAA National Centers for Environmental Information, and Remote Sensing Systems); and the European Centre for Medium-Range Weather Forecasts (ECMWF) and the Copernicus Climate Change Service for ERA5.

Generative artificial intelligence (AI; Anthropic Claude Opus 4.7 Max) was used to manage and orchestrate the complex suite of R and Python scripts underpinning this analysis, including organising the operating environment and associated working directories, documenting scripts extensively, refactoring and optimising code, implementing parallel-processing workflows, and batch processing across multiple SST product lines. AI was also used to produce tables and figures in a manner that integrated these outputs seamlessly within the LaTeX documents, namely the main manuscript and Supplement, and to provide text-shortening and a final editorial pass for grammar and syntax prior to manuscript submission.

Financial support. This research was conducted under the financial support of the National Research Foundation (NRF) of South Africa: Effect of Coastal Ocean Extremes (ECOE), ESS240501216867.

Review statement. This paper was edited by Bernadette Sloyan and reviewed by three anonymous referees.

References

Abrahams, A., Schlegel, R., and Smit, A.: Variation and Change of Upwelling Dynamics Detected in the World's Eastern Boundary Upwelling Systems, Frontiers in Marine Science, 8, 626411, https://doi.org/10.3389/fmars.2021.626411, 2021a.

Abrahams, A., Schlegel, R. W., and Smit, A. J.: A novel approach to quantify metrics of upwelling intensity, frequency and duration, PLOS ONE, 16, https://doi.org/10.1371/journal.pone.0254026, 2021b.

Bai, J. and Perron, P.: Estimating and testing linear models with multiple structural changes, Econometrica, 66, 47–78, https://doi.org/10.2307/2998540, 1998.

Bakun, A.: Coastal Upwelling Indices, West Coast of North America, 1946–71, NOAA Technical Report NMFS SSRF-671, U.S. Department of Commerce, NOAA, National Marine Fisheries Service, Seattle, Washington, https://repository.library.noaa.gov/view/noaa/9041 (last access: 19 November 2026), 1973.

Banzon, V., Smith, T. M., Chin, T. M., Liu, C., and Hankins, W.: A long-term record of blended satellite and in situ sea-surface temperature for climate monitoring, modeling and environmental studies, Earth Syst. Sci. Data, 8, 165–176, https://doi.org/10.5194/essd-8-165-2016, 2016.

Belonenko, T. V., Budyansky, M. V., Akhtyamova, A. F., and Udalov, A. A.: Investigation of the Benguela upwelling eddies using Lagrangian modeling methods, Ocean Dynam., 74, 373–390, 2024.

Benazzouz, A., Pelegrí, J. L., Demarcq, H., Machín, F., Mason, E., Orbi, A., Peña-Izquierdo, J., and Soumia, M.: On the temporal memory of coastal upwelling off NW Africa, J. Geophys. Res.-Oceans, 119, 6356–6380, https://doi.org/10.1002/2013jc009559, 2014a.

Benazzouz, A., Mordane, S., Orbi, A., Chagdali, M., Hilmi, K., Atillah, A., Pelegrí, J. L., and Demarcq, H.: An improved coastal upwelling index from sea surface temperature using satellite-based approach: the case of the Canary Current upwelling system, Cont. Shelf Res., 81, 38–54, https://doi.org/10.1016/j.csr.2014.03.012, 2014b.

Bograd, S. J., Schroeder, I., Sarkar, N., Qiu, X., Sydeman, W. J., and Schwing, F. B.: Phenology of coastal upwelling in the California Current, Geophys. Res. Lett., 36, L01602, https://doi.org/10.1029/2008GL035933, 2009.

Bordbar, M. H., Mohrholz, V., and Schmidt, M.: The relation of wind-driven coastal and offshore upwelling in the Benguela Upwelling System, J. Phys. Oceanogr., 51, 3117–3133, 2021.

Brandt, P., Bordbar, M. H., Coelho, P., Imbol Koungue, R. A., Körner, M., Lamont, T., Lübbecke, J. F., Mohrholz, V., Prigent, A., Roch, M., Schmidt, M., van der Plas, A. K., and Veitch, J.: Physical drivers of Southwest African coastal upwelling and its response to climate variability and change, in: Sustainability of southern African ecosystems under global change: Science for management and policy interventions, 221–257, Springer, https://doi.org/10.1007/978-3-031-10948-5_9, 2024.

Brink, K., Halpern, D., Huyer, A., and Smith, R.: The physical environment of the Peruvian upwelling system, Prog. Oceanogr., 12, 285–305, 1983.

Burnham, K. P. and Anderson, D. R.: Multimodel inference: understanding AIC and BIC in model selection, Sociol. Method. Res., 33, 261–304, 2004.

Byrt, T., Bishop, J., and Carlin, J. B.: Bias, prevalence and kappa, J. Clin. Epidemiol., 46, 423–429, https://doi.org/10.1016/0895-4356(93)90018-V, 1993.

Calvert, S. E. and Price, N. B.: Upwelling and nutrient regeneration in the Benguela Current, October, 1968, Deep-Sea Res. Oceanogr. Abstr., 18, 505–523, https://doi.org/10.1016/0011-7471(71)90074-X, 1971.

Chan, C.-T., Cheong, H.-F., and Shankar, N. J.: A boundary-fitted grid model for tidal motions: orthogonal coordinates generation in 2-D embodying Singapore coastal waters, Comput. Fluids, 23, 881–893, 1994.

Chelton, D. B.: Effects of sampling errors in statistical estimation, Deep-Sea Res. Pt. A, 30, 1083–1103, https://doi.org/10.1016/0198-0149(83)90062-6, 1983.

Chen, Z., Yan, X.-H., Jo, Y.-H., Jiang, L., and Jiang, Y.: A study of Benguela upwelling system using different upwelling indices derived from remotely sensed data, Cont. Shelf Res., 45, 27–33, 2012.

Chicco, D. and Jurman, G.: The advantages of the Matthews correlation coefficient (MCC) over F1 score and accuracy

in binary classification evaluation, BMC Genomics, 21, 6, https://doi.org/10.1186/s12864-019-6413-7, 2020.

de Szoeke, R. A. and Richman, J. G.: On wind-driven mixed layers with strong horizontal gradients – A theory with application to coastal upwelling, J. Phys. Oceanogr., 14, 364–377, https://doi.org/10.1175/1520-0485(1984)014<0364:OWDMLW>2.0.CO;2, 1984.

Gordon, A. L., Bosley, K. T., and Aikman III, F.: Tropical Atlantic water within the Benguela upwelling system at 27° S, Deep-Sea Res. Pt. I, 42, 1–12, 1995.

Hagen, E., Feistel, R., Agenbag, J. J., and Ohde, T.: Seasonal and interannual changes in intense Benguela upwelling (1982–1999), Oceanol. Acta, 24, 557–568, 2001.

Hersbach, H., Bell, B., Berrisford, P., Hirahara, S., Horányi, A., Muñoz-Sabater, J., Nicolas, J., Peubey, C., Radu, R., Schepers, D., Simmons, A., Soci, C., Abdalla, S., Abellan, X., Balsamo, G., Bechtold, P., Biavati, G., Bidlot, J., Bonavita, M., De Chiara, G., Dahlgren, P., Dee, D., Diamantakis, M., Dragani, R., Flemming, J., Forbes, R., Fuentes, M., Geer, A., Haimberger, L., Healy, S., Hogan, R. J., Hólm, E., Janisková, M., Keeley, S., Laloyaux, P., Lopez, P., Lupu, C., Radnoti, G., de Rosnay, P., Rozum, I., Vamborg, F., Villaume, S., and Thépaut, J.-N.: The ERA5 global reanalysis, Q. J. Roy. Meteor. Soc., 146, 1999–2049, https://doi.org/10.1002/qj.3803, 2020.

Hersbach, H., Bell, B., Berrisford, P., Biavati, G., Horányi, A., Muñoz Sabater, J., Nicolas, J., Peubey, C., Radu, R., Rozum, I., and Schepers, D.: ERA5 hourly data on single levels from 1940 to present, Copernicus Climate Change Service (C3S) Climate Data Store (CDS) [data set], https://doi.org/10.24381/cds.adbb2d47, 2023.

Hurvich, C. M. and Tsai, C.-L.: Regression and time series model selection in small samples, Biometrika, 76, 297–307, https://doi.org/10.1093/biomet/76.2.297, 1989.

Hutchings, L., van der Lingen, C. D., Shannon, L. J., Crawford, R. J. M., Verheye, H. M. S., Bartholomae, C. H., van der Plas, A. K., Louw, D., Kreiner, A., Ostrowski, M., Fidel, Q., Barlow, R. G., Lamont, T., Coetzee, J., Shillington, F., Veitch, J., Currie, J. C., and Monteiro, P. M. S.: The Benguela current: An ecosystem of four components, Prog. Oceanogr., 83, 15–32, https://doi.org/10.1016/j.pocean.2009.07.046, 2009.

Iles, A. C., Gouhier, T. C., Menge, B. A., Stewart, J. S., Haupt, A. J., and Lynch, M. C.: Climate-driven trends and ecological implications of event-scale upwelling in the California Current System, Glob. Change Biol., 18, 783–796, https://doi.org/10.1111/j.1365-2486.2011.02567.x, 2012.

Kämpf, J. and Chapman, P.: The Benguela Current upwelling system, in: Upwelling Systems of the World: A Scientific Journey to the Most Productive Marine Ecosystems, 251–314, Springer, https://doi.org/10.1007/978-3-319-42524-5_7, 2016.

Lamont, T., Hutchings, L., van den Berg, M. A., Goschen, W. S., and Barlow, R. G.: Hydrographic variability in the St. Helena Bay region of the southern Benguela ecosystem, J. Geophys. Res.-Oceans, 120, 2920–2944, https://doi.org/10.1002/2014JC010619, 2015.

Lamont, T., García-Reyes, M., Bograd, S., Van Der Lingen, C., and Sydeman, W.: Upwelling indices for comparative ecosystem studies: Variability in the Benguela Upwelling System, J. Marine Syst., 188, 3–16, 2018.

Liu, X., Ma, J., Xu, S., and Wang, B.: On the generation of coastline-following grids for ocean models – trade-off between orthogonality and alignment to coastlines, Ocean Dynam., 67, 1095–1104, 2017.

Lutjeharms, J. and Meeuwis, J.: The extent and variability of South-East Atlantic upwelling, S. Afr. J. Marine Sci., 5, 51–62, https://doi.org/10.2989/025776187784522621, 1987.

Lutjeharms, J. and Valentine, H.: Water types and volumetric considerations of the South-East Atlantic upwelling regime, S. Afr. J. Marine Sci., 5, 63–71, 1987.

Marcello, J., Hernandez-Guerra, A., Eugenio, F., and Fonte, A.: Seasonal and temporal study of the northwest African upwelling system, Int. J. Remote Sens., 32, 1843–1859, https://doi.org/10.1080/01431161003631576, 2011.

Matthews, B. W.: Comparison of the predicted and observed secondary structure of T4 phage lysozyme, Biochim. Biophys. Acta, 405, 442–451, https://doi.org/10.1016/0005-2795(75)90109-9, 1975.

Maturi, E., Sapper, J., Harris, A. and Mittaz, J.: GHRSST level 4 OSPO global foundation sea surface temperature analysis (GDS version 2), National Oceanographic Data Center, NOAA [data set], https://doi.org/10.5067/GHGPB-4FO02, 2014.

Maturi, E., Harris, A., Mittaz, J., Sapper, J., Wick, G., Zhu, X., Dash, P., and Koner, P.: A new high-resolution sea surface temperature blended analysis, B. Am. Meteorol. Soc., 98, 1015–1026, 2017.

Murray, R. J.: Explicit generation of orthogonal grids for ocean models, J. Comput. Phys., 126, 251–273, 1996.

NASA/JPL: GHRSST Level 4 MW_OI Global Foundation Sea Surface Temperature analysis version 5.1 from REMSS, National Oceanographic Data Center, NOAA [data set], https://doi.org/10.5067/GHMWO-4FR51, 2017.

NASA/JPL: GHRSST Level 4 AVHRR_OI Global Blended Sea Surface Temperature Analysis (GDS2), National Oceanographic Data Center, NOAA [data set], https://doi.org/10.5067/GHAAO-4BC21, 2020.

NASA/JPL: GHRSST Level 4 OSTIA Global Historical Reprocessed Foundation Sea Surface Temperature Analysis produced by the UK Meteorological Office, NASA Physical Oceanography Distributed Active Archive Center [data set], https://doi.org/10.5067/GHOST-4RM02, 2023.

Nykjaer, L. and Van Camp, L.: Seasonal and interannual variability of coastal upwelling along northwest Africa and Portugal from 1981 to 1991, J. Geophys. Res.-Oceans, 99, 14197–14207, https://doi.org/10.1029/94JC00814, 1994.

Pavlushin, V. A. and Kubryakov, A. A.: Variability of the area and shape of the Benguela upwelling in 1985–2017 and its relation with dynamic characteristics from satellite measurements, Izvestiya, Atmos. Ocean. Phys., 58, 1037–1048, https://doi.org/10.1134/S0001433822090183, 2022.

Salama, A. T., Lovato, T., Butenschön, M., and Zavatarelli, M.: A coupled physical–biogeochemical modeling approach to investigate the dynamics of the Benguela Upwelling System, Frontiers in Marine Science, 12, 1601284, https://doi.org/10.3389/fmars.2025.1601284, 2025.

Santos, A., Kazmin, A., and Peliz, A.: Decadal changes in the Canary upwelling system as revealed by satellite observations: their impact on productivity, J. Mar. Res., 63, 359–379, 2005.

Schwarz, G.: Estimating the dimension of a model, Ann. Stat., 6, 461–464, https://doi.org/10.1214/aos/1176344136, 1978.

Seabra, R., Varela, R., Santos, A. M., Gómez-Gesteira, M., Meneghesso, C., Wethey, D. S., and Lima, F. P.: Reduced nearshore warming associated with Eastern Boundary Upwelling Systems, Frontiers in Marine Science, 6, 104, https://doi.org/10.3389/fmars.2019.00104, 2019.

Smit, A. J. and Sweijd, N. A.: A segmented-breakpoint measure of cross-shore sea-surface-temperature structure in the Benguela system: code and derived data, version 1.0.0, Zenodo [code, data set], https://doi.org/10.5281/zenodo.24306305, 2026.

Spekreijse, S. P.: Elliptic grid generation based on Laplace equations and algebraic transformations, J. Comput. Phys., 118, 38–61, 1995.

Tomety, F. S., Illig, S., Ostrowski, M., Awo, F. M., Bachèlery, M.-L., Keenlyside, N., and Rouault, M.: Long-term climatological trends driving the recent warming along the Angolan and Namibian coasts, Clim. Dynam., 62, 7763–7782, https://doi.org/10.1007/s00382-024-07305-z, 2024.

UKMO: GHRSST Level 4 OSTIA global foundation sea surface temperature analysis (GDS version 2), NASA Physical Oceanography Distributed Active Archive Center [data set], https://doi.org/10.5067/GHOST-4FK02, 2013.

Vasquez-Cuervo, J., Dewitte, B., Chin, T. M., Armstrong, E. M., Purca, S., and Alburqueque, E.: An analysis of SST gradients off the Peruvian coast: the impact of going to higher resolution, Remote Sens. Environ., 131, 76–84, https://doi.org/10.1016/j.rse.2012.12.010, 2013.

Wentz, F. J. and Meissner, T.: AMSR Ocean Algorithm, Algorithm Theoretical Basis Document, Version 2, RSS Tech. Proposal 121599A-1, Remote Sensing Systems, Santa Rosa, CA, 59 pp., https://images.remss.com/papers/rsstech/2000_121599A-1_Wentz_AMSR_Ocean_ATBD_V2.pdf (last access: 19 November 2026), 2000.

Worsfold, M., Good, S., Atkinson, C., and Embury, O.: Presenting a long-term, reprocessed dataset of global sea surface temperature produced using the OSTIA system, Remote Sens., 16, 3358, https://doi.org/10.3390/rs16183358, 2024.

Yao, Y.-C.: Estimating the number of change-points via Schwarz' criterion, Stat. Probabil. Lett., 6, 181–189, https://doi.org/10.1016/0167-7152(88)90118-6, 1988.

Zhang, N. R. and Siegmund, D. O.: A modified Bayes information criterion with applications to the analysis of comparative genomic hybridization data, Biometrics, 63, 22–32, https://doi.org/10.1111/j.1541-0420.2006.00662.x, 2007.